Journal of Materials Chemistry C

ROYAL SOCIETY OF CHEMISTRY

PAPER

View Article Online
View Journal | View Issue

Cite this: J. Mater. Chem. C, 2021, 9, 15074

On the stability of calcium and cadmium based Ruddlesden–Popper and double perovskite structures†

Michel L. Marcondes, *[a] Samuel S. M. Santos, [b] Ivan P. Miranda, [a] Pedro Rocha-Rodrigues, [b] Lucy V. C. Assali, [a] Armandina M. L. Lopes, [b] João P. Araújo [b] and Helena M. Petrilli [a]

Received 20th August 2021,
Accepted 1st October 2021

DOI: 10.1039/d1tc03947d

rsc.li/materials-c

This paper presents *ab initio* calculations on stability properties and phase diagrams of Ca- and Cd-related hybrid improper ferroelectric materials, with the Ruddlesden–Popper (RP) and double perovskite (DP) structures. The results show that enthalpy relations favor the decomposition of Cd-based RP compounds, indicating that experimental synthesis may be nontrivial. Thus, pure Cd-related RP compounds are not stable. The RP $Ca_3B_2O_7$ (B = Ti, Mn) systems, however, admit the incorporation of certain percentages of Cd replacing Ca, providing a possible route for tuning ferroelectric properties through chemical substitution. In addition, the stability results indicate that the Ca_2TiO_4 RP is not stable, in agreement with previous investigations. Searching for alternative stable phases, we found that the forsterite structure might be stable at room temperature and a new structure for this material. Moreover, the results reveal that the Cd-based DP $CaCdTi_2O_6$ is dynamically stable, therefore, a possible new hybrid improper ferroelectric.

1 Introduction

Hybrid improper ferroelectricity occurs in Ruddlesden–Popper (RP) and double perovskite (DP) structures.[1] The octahedral rotations that accompany this kind of ferroelectricity can couple to magnetic moments,[2] opening new routes for magneto-electric control. Although proper ferroelectrics have been used in capacitors and random access memories (RAM),[3] hybrid improper ferroelectrics (HIF) have not encountered the same room for applications. The main reasons are the lack of HIF with high polarization and the large coercive field for polarization switching, the latter being critical for memory usages.[4] Currently, few HIF are known so that the hunt for adequate new materials for technological applications is an active topic of research. Caused by a relative displacement between negative and positive centers, spontaneous electric polarization requires the break of inversion symmetry. Because of the small number of space groups that allow this kind of symmetry breaking, HIF materials are scarce. Accordingly, the design of new compounds relies on using, as building blocks, materials at which space group symmetry allows ferroelectric transition. Known materials inspire the design of new compounds, and specific chemical modifications can tune properties such as electric polarization and energy barriers.[5–7]

With the chemical formula $A_{n+1}B_nO_{3n+1}$, the RP structure is formed by inserting a rock-salt layer between n stacked perovskite blocks.[8] Examples of RP with n = 2 (RP2) are the $Ca_3Mn_2O_7$ and $Ca_3Ti_2O_7$ compounds, while Ca_2MnO_4 is an example of a RP with n = 1 (RP1). Not all elements of the RP series are HIF. Group theoretical methods have shown that hybrid improper ferroelectricity occurs if n is even, but inhibited if n is odd.[9]

Previously, we have shown that Cd embeds in the Ca sites of RP structures.[10,11] Using *ab initio* calculations, we demonstrated how these substitutions affect the octahedral distortions and ferroelectric properties of the $Ca_3Ti_2O_7$ and $Ca_3Mn_2O_7$.[7] Furthermore, we showed that a quadratic relationship between the main component of the electric field gradient tensor holds for HIF perovskite phase transtions.[12] Nevertheless, an important question that remained to be answered is how such cation substitution affects the stability of Ca-based RP1 and RP2 crystals, issue that is one of the main goals of the current investigation.

Although non-centrosymmetric RP1 structures are scarce,[9] properties such as negative thermal expansion have attracted attention to these materials. The RP1 Ca_2MnO_4 has already been synthesized, and recent experimental measurements combined with *ab initio* calculations have shown its high-temperature structural phase transitions and enhancement of uniaxial

[a] Universidade de São Paulo, Instituto de Física, Rua do Matão, 1371, 05508-090, São Paulo, SP, Brazil. E-mail: michel@if.usp.br
[b] IFIMUP, Institute of Physics for Advanced Materials, Nanotechnology and Photonics, Departamento de Física e Astronomia da Faculdade de Ciências da Universidade do Porto, Rua do Campo Alegre, 687, 4169-007 Porto, Portugal

† Electronic supplementary information (ESI) available. See DOI: 10.1039/d1tc03947d

negative thermal expansion.[11] Therefore, the search for the analogous RP1 Ca_2TiO_4 should be inspired by the analogy between $Ca_3Mn_2O_7$ and $Ca_3Ti_2O_7$ compounds. Still, theoretical studies have indicated that RP $Ca_{n+1}Ti_nO_{3n+1}$ are stable only for $n > 1$.[13] Predicting correct stability requires accurate knowledge of the crystal structure, and the Ramadan *et al.*[13] investigation used crystallographic structures based on other known RP1 compounds rather than the analogous Ca_2MnO_4. Thus, stable crystals with the chemical formula Ca_2TiO_4 belonging to other space groups should not be discarded, and we searched for Ti-based stable compounds having in mind the above statements.

The *Pnma* perovskite is an important structure used as a scaffolding to construct new HIF with the DP structure.[2,14] In this space group, the A-site cation of the ABO_3 perovskite occupies the 4c Wyckoff position. By replacing two of the four A-atoms in the unit cell, one can break the inversion symmetry. These atomic substitutions generate the $AA'B_2O_6$ DP structure with the space group $Pmc2_1$.[2,7,14] In the *Pnma* perovskite space group, the A-site cation possesses anti-polar displacement, and inversion symmetry ensures that no electric polarization arises. Conversely, in the DP structure, the anti-displacements are not equal due to the lack of inversion symmetry, which generates a spontaneous electric polarization. Good elemental block candidates for building DP materials are the $CaTiO_3$ and $CaMnO_3$ perovskites since they stabilize in the suitable *Pnma* space group. Indeed, our theoretical calculations for the DP $CaCdB_2O_6$ (B = Ti, Mn) predicted energy barriers slightly larger than those of the RP2 $Ca_3Mn_2O_7$ compound and electric polarization of the same order.[7] However, the thermal and dynamical stabilities of these DPs remained an open question that we will address here.

This work presents theoretical calculations on the phase stability of Ti- and Mn-based RP and DP materials. By computing the relative enthalpy, we provide a concentration range for Cd atoms in the RP structures. Also, we inspect the dynamical and thermal stability of compounds with chemical formula A_2BO_4 (A = Ca, Cd and B = Ti, Mn).

2 Methodology

The *ab initio* calculations were performed with the Quantum ESPRESSO computational package[15,16] in the framework of the density functional theory (DFT).[17,18] Computational details can be found in the ESI.† Also, the relation between octahedral rotation and tilts with the polar structure formation was addressed elsewhere.[7,12] For each structure, we calculated the equation of state (EOS) parameters by optimizing the crystal cell at ten different pressures using the variable cell shape molecular dynamics[19,20] and fitting the third-order Birch-Murnaghan EOS:[21]

$$E(V) = E_0 + \frac{9V_0K_0}{16}\times\left\{\left[\left(\frac{V_0}{V}\right)^{\frac{2}{3}}-1\right]^3 K_0' + \left[\left(\frac{V_0}{V}\right)^{\frac{2}{3}}-1\right]^2\left[6-4\left(\frac{V_0}{V}\right)^{\frac{2}{3}}\right]\right\} \quad (1)$$

where E_0, V_0, K_0, and K_0' are the energy, volume, bulk modulus, and bulk modulus pressure derivative, respectively, at null pressure. Then, the enthalpy H is given by:

$$H = E + PV, \quad (2)$$

where E is the energy, P the pressure, and V the volume. To predict the most stable structure, we compute the enthalpy as a function of pressure for each component present in the possible dissociation chemical reaction. Because RPn phases are constructed by a rock-salt layer positioned between n ABO_3 perovskite blocks, one possible chemical reaction is the dissociation into their n respective perovskites plus one rock-salt crystal. In addition, the ABO_3 single block can decompose into a rock-salt system plus an oxide of the BO_2 type. Therefore, for the RPn compounds, we consider the following chemical reactions:

$$A_{n+1}B_nO_{3n+1} \leftrightarrow nABO_3 + AO; \quad (3)$$

$$A_{n+1}B_nO_{3n+1} \leftrightarrow (n-1)ABO_3 + BO_2 + 2AO; \quad (4)$$

$$A_{n+1}B_nO_{3n+1} \leftrightarrow (n+1)AO + nBO_2. \quad (5)$$

Following these reactions schemes, we computed the relative enthalpies for the RPn perovskites of the type $A_{n+1}B_nO_{3n+1}$, with $n = 1$ and $n = 2$, where A = Cd, Ca and B = Ti, Mn. Moreover, we performed similar calculations considering the RP2 $Ca_3B_2O_7$ crystals with Cd substituting Ca ions at the rock-salt site only, *i.e.*, the materials with chemical formula $CaCd_2B_2O_7$.

Regarding the DP structures, they can decompose into two single perovskite structures. Additionally, each perovskite can be further decomposed into simpler systems so that the following four chemical reactions are possible:

$$AA'B_2O_6 \leftrightarrow ABO_3 + A'BO_3; \quad (6)$$

$$AA'B_2O_6 \leftrightarrow ABO_3 + A'O + BO_2; \quad (7)$$

$$AA'B_2O_6 \leftrightarrow A'BO_3 + AO + BO_2; \quad (8)$$

$$AA'B_2O_6 \leftrightarrow AO + A'O + 2BO_2. \quad (9)$$

We followed these reactions to compute the relative enthalpies of the DP structures composed of Ca and Cd ions with chemical formula $CaCdB_2O_6$ where B = Ti, Mn.

To describe the RP2 systems, we used the $A2_1am$ space group since this is the known low-temperature structure not only for $Ca_3Mn_2O_7$, but also for other known RP2 crystals.[22,23] For the DP structures, we used the $Pmc2_1$ space group, obtained replacing two A-site atoms in the *Pnma* structure.

The $CaBO_3$ compounds were simulated in the *Pnma* perovskite structure since this is their ground state phase, while for $CdTiO_3$ compounds the $R\bar{3}$ space group was used because they stabilize in the ilmenite structure.[24] The $R\bar{3}$ space group was also used to describe the $CdMnO_3$ system.

The MnO_2 and TiO_2 oxides have the pyrolusite and the rutile crystal structures, respectively, both belonging to the $P4_2/mnm$ space group. The TiO_2 was simulated in both, anatase and rutile, structures, and the results reported here are for the rutile

one. The total energy difference between these two phases is negligible and does not affect our conclusions.

Theoretical calculations complemented with experimental evidence showed that Ca_2MnO_4 may coexist in $I4_1/acd$ and *Acam* space groups.[11] Thus, RP1 systems were calculated in both structures and the *Acam* phase displayed lower total energy than $I4_1/acd$. Consequently, we used the *Acam* ground state phase to study the chemical reactions of the RP1 phases. Additionally, because the forsterite and RP1 perovskite crystals have identical chemical formulas, we also investigated the stability properties taking into account the *Pnma* space group. Fig. 1 shows schematic representations of all structures studied here.

Table 1 Equation of state parameters for the $A_3B_2O_7$ (A = Ca, Cd and B = Mn, Ti) RP2 systems. SG is the ground state space group, SG (#) is the spacial group number,[a] V_0 is the equilibrium volume (Å^3), K_0 the bulk modulus (GPa), and K_0' the bulk modulus pressure derivative (dimensionless)

System	SG	SG (#)	V_0	K_0	K_0'
$Ca_3Mn_2O_7$	$A2_1'am'$	36.174	272.63	146.8	4.44
$CaCd_2Mn_2O_7$	$A2_1'am'$	36.174	271.74	158.6	4.30
$Cd_3Mn_2O_7$	$A2_1am$	36.172	272.22	160.8	4.50
$Ca_3Ti_2O_7$	$A2_1am$	36	294.27	137.4	4.62
$CaCd_2Ti_2O_7$	$A2_1am$	36	291.28	138.4	5.13
$Cd_3Ti_2O_7$	$A2_1am$	36	291.82	131.2	5.87

[a] International tables for crystallography.

3 Results and discussion

3.1 Ruddlesden–Popper phases

3.1.1 RP2 structures. Table 1 shows the EOS parameters of the $A_3B_2O_7$ (A = Ca, Cd and B = Mn, Ti) RP2 compounds. The Mn-based materials are antiferromagnetic, and the table shows the magnetic space groups corresponding to the magnetic ground state. The EOS parameters of the respective single perovskites, rock-salt oxides, and BO_2 systems, necessary to compute the phase transitions, are depicted in Table S1 of the ESI.† The bulk moduli are in the 105–225 GPa range. In general, Ti-based structures have larger volumes, resulting in smaller bulk moduli than the respective Mn-based systems. The larger atomic radius of Ti, compared to Mn, increases the BO_6 octahedra bond distances by around 3.5% and causes the bulk moduli reduction. As shown in Fig. S1 of the ESI,† the RP2 EOSs

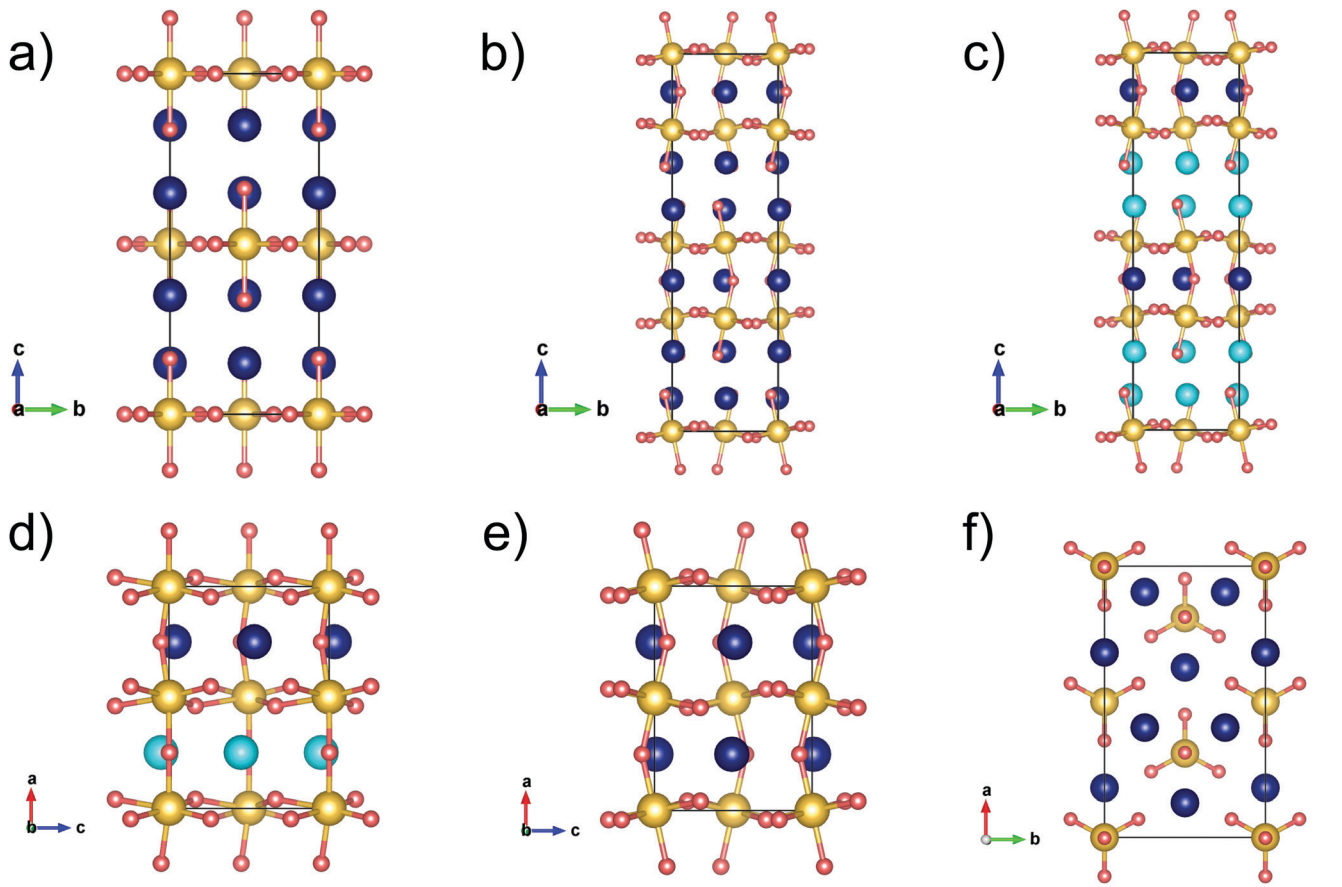

Fig. 1 Schematic representations of the main structures considered in the enthalpy calculations. Orange, yelow, dark blue, and light blue spheres represent oxygen-site, B-site, A-site, and A′-site, respectively. (a) *Acam* (RP1); (b) and (c) $A2_1am$ (RP2); (d) $Pmc2_1$ (DP); (e) *Pnma* (single perovskite); (f) *Pnma* (forsterite).

divide into two groups: one for Ti-based and another for Mn-based systems. The Ca by Cd substitution is akin. Since Cd is slightly smaller than Ca, the Cd–O mean distance is smaller than the Ca–O. Barely affecting the crystal volumes in Mn-related systems, this effect is more pronounced in Ti-based compounds.

Fig. 2a shows the relative enthalpy, per formula unit (f.u.), for the Mn- and Ti-based RP2 materials, with respect to the $A2_1am$ space group, depicted in the figure by the solid black line at 0 eV. Only dissociations with the lowest enthalpies are shown; all possible chemical reactions, as proposed in the Methodology, are displayed in Fig. S2 of the ESI.† With the lowest relative enthalpies at ambient pressure, the Ca-based RP2 structures are stable against dissociations. The $Ca_3Mn_2O_7$ compound is stable up to $\sim$11 GPa, dissociating into $2CaMnO_3$ + CaO at higher pressures. The larger ionic radius of Ti, compared to Mn, decreases the pressure of the $Ca_3Ti_2O_7 \rightarrow 2CaTiO_3$ + CaO dissociation reaction to around 0.5 GPa. This low transition pressure might explain the experimentally observed degradation of $Ca_3Ti_2O_7$ samples at high temperatures.[22] All transitions present in the Mn-based systems are also present in the Ti-based ones, but at lower pressures (see Fig. S2 of the ESI†).

According to Fig. 2, starting from the $Cd_3B_2O_7$ dissociation reaction to the $Ca_3B_2O_7$ one, passing through $CaCd_2B_2O_7$, the enthalpy difference w.r.t. the RP2 structure decreases. Whence, the higher concentration of calcium favors the formation of these compounds, meaning that Ca atoms assist in stabilizing Cd-related RP2 structures. As a result, even thought pure Cd-based compounds dissociate, the Ca-based RP2 materials might incorporate a certain amount of Cd ions replacing Ca in the crystal structure. Showing that Cd impurities occupy the rock-salt site of $Ca_3Mn_2O_7$, PAC experiments support this conclusion.[10] Controlling Cd concentration may be a route to tailor ferroelectric properties through chemical substitution; however, a question arises: what is the maximum Cd concentration at which the structure is still stable? To provide an answer, we proceed in two steps: firstly, we interpret the RP2 structures as solid solutions of the type $Ca_{3(1-x)}Cd_{3x}B_2O_7$, so that if $x = 1$ ($x = 0$) the structure corresponds to $Cd_3B_2O_7$ ($Ca_3B_2O_7$); secondly, we compute the enthalpy difference between the RP2 compound and the respective dissociation in simpler crystals as a function of the Cd concentration x. The structures studied here, namely $Ca_3B_2O_7$, $CaCd_2B_2O_7$, and $Cd_3B_2O_7$, correspond to $x = 0.00$, 0.67, and 1.00, respectively. Fig. 3 shows that, as x increases, the difference decreases, with the RP2 being stable up to $x = 0.20$ when B = Mn and up to $x = 0.07$ when B = Ti. To further confirm the adopted model to obtain the Cd doping limitation into the RP2 structures, Fig. S3 of the ESI† displays a comparison of the fitting procedure with *ab initio* calculations results, obtained by replacing the Ca by Cd in all possible positions of the $Ca_3Ti_2O_7$ primitive cell.

Our results indicate that Mn-based Ca–Cd compounds should be easier to be synthesized than those based on Ti. Moreover, these results provide what would be the favorable conditions to grow these RP2 materials. Using the supercell scheme, we simulate the Ti-based system with a Cd concentration $x \approx 0.067$, *i.e.*, the $Ca_{2.80}Cd_{0.20}Ti_2O_7$ compound, we obtained a standard enthalpy of formation $\Delta_f H^0 = -2.76$ Ry. Comparing this value with $\Delta_f H^0 = -2.78$ Ry, the standard enthalpy of formation acquired for the $Ca_3Ti_2O_7$ system, we can perceive a higher $\Delta_f H^0$ when Cd is in the structure, indicating that the incorporation of Cd decreases the overall stability, as predicted by our dissociation model, and that the formation of these compounds is exothermic.

3.1.2 RP1 structures. The RP1 Ca_2MnO_4 has already been synthesized, and PAC experiments have probed its local order *via* EFG measurements.[11] Because of the similarities between $Ca_3Mn_2O_7$ and $Ca_3Ti_2O_7$ RP2 structures, the existence of

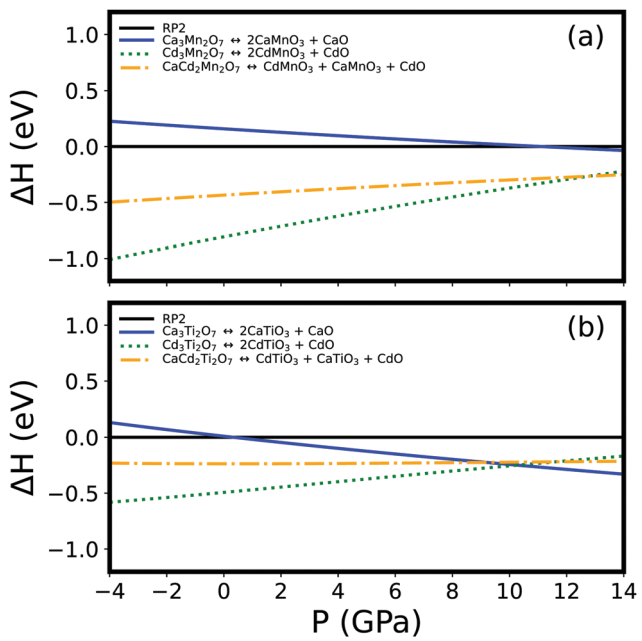

Fig. 2 RP2 relative enthalpy ΔH for the dissociation reactions of (a) Mn-based systems and (b) Ti-based systems, per f.u., w.r.t. the ground state $A2_1am$ space group, represented by the solid black lines at 0 eV.

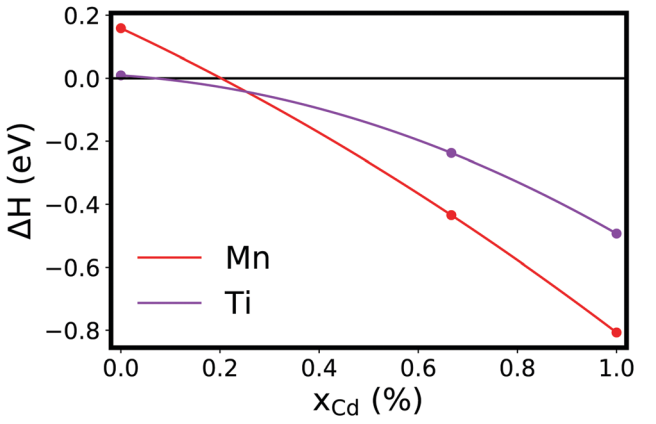

Fig. 3 Enthalpy difference, per f.u., between the RP2 structures (solid black line at 0 eV) and the result of their dissociation into simpler crystals, for the reaction with the lowest enthalpy at 0 GPa, as a function of the percentage of cadmium concentration, for Mn- and Ti-based compounds.

Ca_2MnO_4 motivates the search for similar Ti-based RP1 compounds. Ca_2TiO_4, however, has not been stabilized yet. Previous theoretical calculations have shown that Ti-based RP structures could be stable only for $n > 1$, showing that Ca_2TiO_4 is not stable.[13] These calculations constructed crystal structures for Ca–Ti–O systems based on Sr–Ti–O RP ones. Here, we follow a different approach to simulate the properties of Ca_2TiO_4, using the experimental crystalline structures at which Ca_2MnO_4 stabilizes at ambient pressure.

Neutron diffraction data[11] indicates that Ca_2MnO_4 exhibits two related structural phases: the $I4_1/acd$ and the *Acam* space groups. Therefore, one could extrapolate that Ca_2TiO_4 would also stabilize, for instance, in the RP1 *Acam* structure. We chose to use the *Acam* space group instead of the $I4_1/acd$ because of the former's lower total energy. Nevertheless, the total energy difference between these phases is minimal so that this choice does not affect our main conclusions. Other crystalline structures, however, are also possible. Indeed, RP1 materials have the same stoichiometry as the Mg_2SiO_4 forsterite crystal. Forsterite is the stable structure of the magnesium silicate at ambient pressure and dissociates into $MgSiO_3$ + MgO above 20 GPa. Because $MgSiO_3$ and $CaTiO_3$ are similar systems, with similar structures, it is natural to expect analogous transitions in systems of the type A_2BO_4 (A = Ca, Mg and B = Si, Ti). To investigate this issue, we also computed the EOS of Ca_2TiO_4 with the forsterite crystalline structure, which belongs to the space group *Pnma* but is not related to the single perovskite structure. While the *Pnma* perovskite is built through rotations of the BO_6 octahedra of the $Pm\bar{3}m$ (#221) cubic perovskite, the B-site cation in forsterite occupies a tetrahedral BO4 site, as shown in Fig. 1(f).

Table 2 shows the EOS parameters for A_2BO_4 (A = Ca, Cd and B = Ti, Mn) compounds in the *Acam* (RP1) and *Pnma* (forsterite) space groups (see Fig. S4 of the ESI†). The crystal volumes are larger for the forsterite phase than for the RP1 structure; consequently, forsterite has smaller bulk moduli. Fig. 4 displays the enthalpies of A_2BO_4 compounds, relative to the enthalpy of the *Acam* structure. As expected, Ca_2MnO_4 in the *Acam* space group is more favorable than in the *Pnma* phase for the entire pressure range. Conversely, Ca_2TiO_4 with the forsterite *Pnma* space group is the most stable structure up to ≈ 5 GPa, compared to the *Acam* phase. To our knowledge, no previous reports of the Ca_2TiO_4 stability properties with the forsterite crystalline structure exist. Table S2 in the ESI† contains the crystallographic data obtained here for Ca_2TiO_4 in the forsterite structure, and Fig. S5 (ESI†) shows its bandstructure.

Fig. 4(a and b) also show the relative enthalpy between Mn-based and Ti-based structures, respectively, for the A_2BO_4 systems (A = Ca, Cd and B = Ti, Mn), as well as the result of their dissociation into simpler crystals, according to the equations described in the Methodology section. Cd-Based RP1 systems are not favorable against dissociation into $CdBO_3$ + BO_2, as observed by comparing the solid black line and the dark green dotted line in Fig. 4(a and b). The dissociation pressure of Cd_2TiO_4 is around 0 GPa, given by the crossing between the orange and dark green dotted lines in Fig. 4(b), suggesting that it could be thermodynamically stable; however, the phonon dispersion spectrum presents imaginary frequencies in some branches, indicating that Cd_2TiO_4 is dynamically unstable (see Fig. S6 of the ESI†). Regarding Ca-based materials, Ca_2MnO_4 in the *Acam* (RP1) structure does not dissociate, as evidenced by the blue and red lines that are above the black one in Fig. 4(a), in agreement with experiments. For Ti-based materials, our results show that Ca_2TiO_4 does not dissociate, and that the forsterite (*Pnma*) crystal structure presents the lowest enthalpy up to ~ 3 GPa, noticed by the red line in Fig. 4(b). Fig. S7 of the ESI† displays the phonon dispersion curve of the forsterite Ca_2TiO_4 at null pressure, implying that this structure is dynamically stable. Therefore, our results demonstrate a possible stable structure for Ca_2TiO_4.

3.1.3 Relative enthalpy between $A_3B_2O_7$ and A_2BO_4 compounds. An important reaction from the experimental

Table 2 Equation of state parameters for the A_2BO_4 (A = Ca, Cd and B = Mn, Ti) systems with the RP1 (*Acam*) and forsterite (*Pnma*) phases. SG is the space group, V_0 is the equilibrium volume (Å^3), K_0 the bulk modulus (GPa), and K_0' the bulk modulus pressure derivative (dimensionless)

System	SG	SG (#)	V_0	K_0	K_0'
Ca_2MnO_4	*Acam*	64.469	329.88	141.2	4.42
	Pn′ma	62.443	414.72	54.0	4.00
Cd_2MnO_4	*Pc′ma′*[a]	55.537	327.03	153.0	4.82
	Pn′ma	62.443	417.37	39.5	5.81
Ca_2TiO_4	*Acam*	64	353.31	133.7	4.22
	Pnma	62	428.65	61.3	3.05
Cd_2TiO_4	*Acam*	64	349.34	131.6	5.17
	Pnma	62	415.50	75.9	2.43

[a] The antiferromagnetic order breaks the spatial symmetry and transforms the system into the *Pcma* space group.

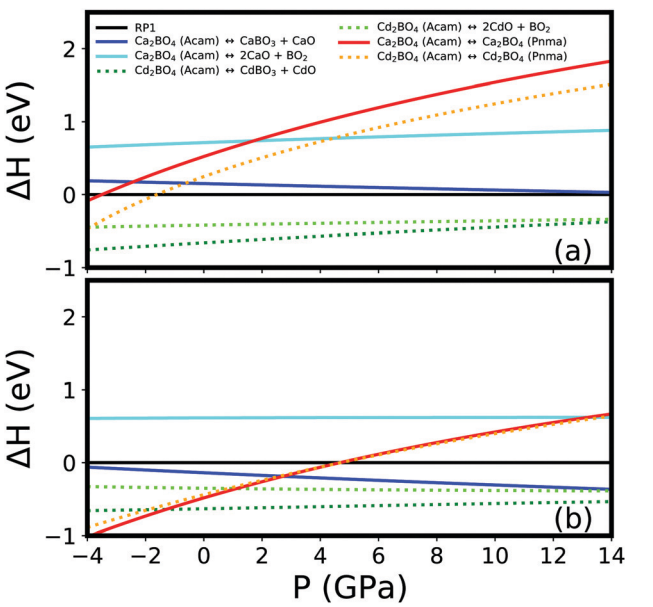

Fig. 4 Relative enthalpies ΔH, per f.u., for the dissociation reactions of Ca_2BO_4 and Cd_2BO_4. (a) B = Mn, (b) B = Ti. ΔH is calculated with respect to the *Acam* phase, represented by the solid black lines at 0 eV. The color conventions are the same for both figures.

perspective not commented so far is the dissociation of the RP2 phase into a RP1 one plus a single perovskite structure:

$$A_3B_2O_7 \leftrightarrow A_2BO_4 + ABO_3. \quad (10)$$

As shown in Fig. 5(a), the small relative enthalpy between $Ca_3Mn_2O_7$ material and the dissociated compounds (solid red lines) indicates that RP2 and RP1 structures may coexist. This result agrees with the experimental observation that the usual synthesis of $Ca_3Mn_2O_7$ by solid state reaction processes, for instance, follows the formation of secondary phases of Ca_2MnO_4 RP1 and $CaMnO_3$ perovskite, and several consecutive grinding and annealing processes are required to achieve a pure $Ca_3Mn_2O_7$ RP2 sample.[10] In addition, the results for Ti-based materials displayed in Fig. 5(b) show a lower enthalpy for the dissociation into forsterite plus perovskite structures (solid red line).

3.2 Double perovskites

The DP is an interesting structure to build novel HIF since it has a similar ferroelectricity mechanism as the RP materials. In single perovskites of the ABO3 type, rotations of the BO6 octahedra allows a displacement of the A-site cations, generating an in-layer polarization. However, the system is centrosymmetric and adjacent layers have opposite displacements, hence the in-layer polarization cancels out. The chemical modification in building the DP structures breaks the inversion symmetry, allowing different displacement magnitudes of these layers, and the system is ferroelectric. This process is similar to that of RP2 systems. Here, the centrosymmetric structure belongs to the space group $Pmc2_1$. Two irreducible representations, corresponding to octahedral distortions, break the inversion symmetry and allows an anti-displacement of the A-site cations, configuring a trilinear coupling.[7,12]

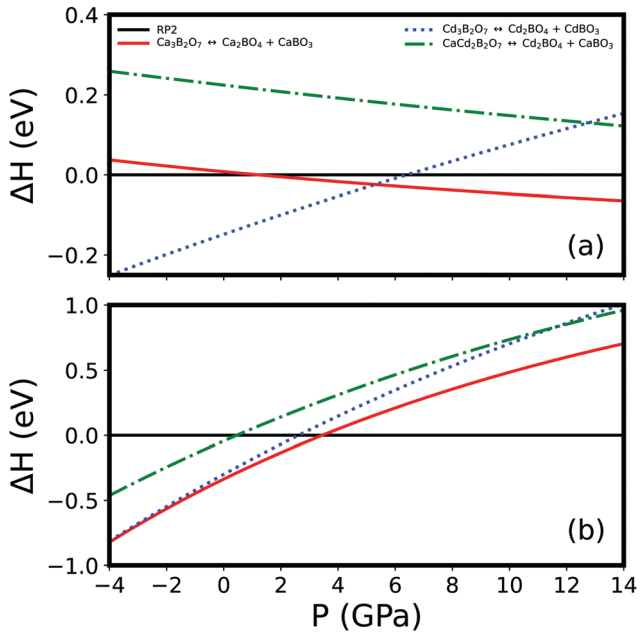

Fig. 5 Relative enthalpies ΔH, per f.u., for the dissociation reactions of RP2 compounds into A_2BO_4 plus ABO_3, A = Ca, Cd. (a) B = Mn; (b) B = Ti. For A_2BO_4, we used the space groups *Acam* and *Pnma*, respectively, for B = Mn and B = Ti. ΔH is calculated w.r.t. the RP2 phase represented by the solid black lines at 0 eV. The color conventions are the same for both figures.

Table 3 shows the EOS parameters for the $AA'B_2O_6$ (A = Ca, Cd and B = Ti, Mn) DP structures. Although the primitive cell of the DP structures have fewer atoms—smaller volumes—than the RP_2 ones, a similar relation between the B-site cation and the crystal volume occurs. The smaller ionic radius of Mn makes the $CaCdMn_2O_6$ cell smaller than the $CaCdTi_2O_6$ one, consequently, here again the bulk modulus of the former is larger than the latter.

Fig. 6 presents the relative enthalpy for the DP structures chemical reactions. Mn-Based DP dissociates into $CaMnO_3$ and $CdMnO_3$ single compounds, *i.e.*, $CaCdMn_2O_6$ could be stable only at high pressures, above 12 GPa, as evidenced by the crossing between the red and black lines in Fig. 6(a). With decreasing pressure, the $CaCdMn_2O_6$ DP dissociation into $CaMnO_3$ + CdO + MnO_2 also has lower enthalpy than the DP phase, as noticed by the crossing between the light blue line with the black one. Therefore, Mn-based DP structures are unlikely to be even metastable at 0 GPa and are not good ferroelectric candidates. Although the Ti-based DP also tends to dissociate into ABO_3 single systems, the DP structure is stable above $\sim$5.2 GPa, given by the crossing between the red and black lines in Fig. 6(b). Therefore, Ti-based DP crystals might be metastable at ambient pressure and could stabilize *via* high-pressure synthesis routes.

As indicated in Fig. S8 of the ESI,† while Ca-based systems have a strong tendency to stabilize in the *Pnma* perovskite structure, CdBO3 materials stabilize in the $R\bar{3}$ space group. Our results show that the DP can stabilize even if one of the ABO_3 systems is not a perovskite structure, in agreement with the guidelines of Rondinelli and Fennie.[25] We have previously shown that $CaCdTi_2O_6$ compound has spontaneous electric polarization and polarization switch energy barriers of the same order of the RP2 $Ca_3Ti_2O_7$ system,[7] thus in the range of experimental observation.[26] Fig. 6 shows that $CaCdTi_2O_6$ is thermally stable. To confirm the dynamical stability, Fig. S9 of the ESI† shows the phonon dispersion curves along high-symmetry directions of the $CaCdTi_2O_6$ first Brillouin zone (BZ). The frequencies are positive along all paths, showing that this structure is also dynamically stable. Our results demonstrate $CaCdTi_2O_6$ as a possible new hybrid improper ferroelectric. The formation enthalpy calculations show that from solid state reaction route, this structure should only be formed at high-pressure. Still, one of the experimental difficulties in

Table 3 Equation of state parameters for the DP structures. SG is the ground state space group, V_0 is the equilibrium volume (Å^3), K_0 the bulk modulus (GPa), and K_0' the bulk modulus pressure derivative (dimensionless)

System	SG	SG (#)	V_0	K_0	K_0'
$CaCdMn_2O_6$	$Pm'c2_1'$	26.68	211.13	181.7	4.49
$CaCdTi_2O_6$	$Pmc2_1$	26	231.65	124.0	6.77

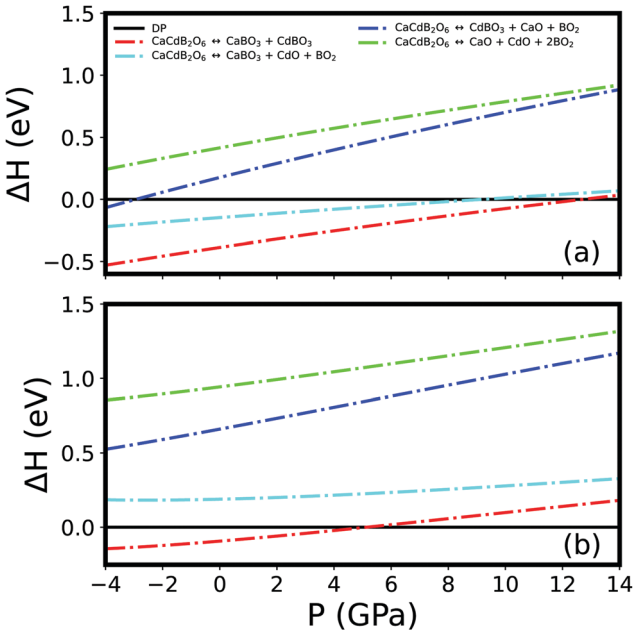

Fig. 6 DP relative enthalpy ΔH, per f.u., for the dissociation reactions, w.r.t. the ground state $Pmc2_1$ space group, represented by the solid black lines at 0 eV, as a function of pressure. (a) B = Mn; (b) B = Ti. The color conventions are the same for both figures.

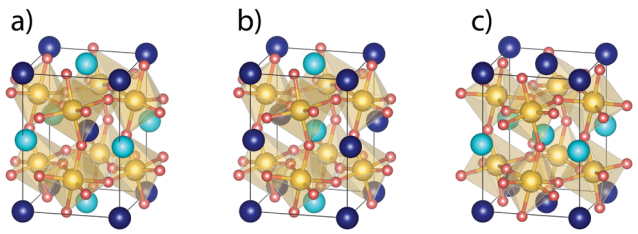

Fig. 7 A-site ordering configurations for DP structures with chemical formula $AA'B_2O_6$. Orange, yellow, dark blue, and light blue spheres represent oxygen-site, B-site, A-site, and A′-site, respectively. (a) Rocksalt ordering; (b) columnar ordering; (c) layered ordering.

synthesizing HIF DP phases is to realize the A-site ordering since some configurations are possible, as shown in Fig. 7, besides the layered structure considered and analyzed so far.

Therefore, we also carried out simulations for the rocksalt and columnar ordering structures. At 0 GPa, rocksalt and columnar ordering have enthalpies 0.17 eV and 0.06 eV above that of layered DP, respectively. Increasing to 0.36 eV (rocksalt) and 0.27 eV (columnar) at 5 GPa, these differences further demonstrate that high pressures favor the layered ordering in these DP structures. Consequently, since the phonon dispersion curves show that $CaCdTi_2O_6$ should be dynamically stable at ambient pressure, such A-site layered perovskite may eventually be synthesized as thin film structures, where sequential deposition of $CaTiO_3$ and $CdTiO_3$ layers can be performed, in a similar manner as the experimental $PbTiO_3$:$SrTiO_3$ supperlattices example, that triggered the discussion of the hybrid improper ferroelectric materials.[27,28] What our results demonstrated is $CaCdTi_2O_6$ as a possible new hybrid improper ferroelectric with the DP structure that could be stabilized *via* high-pressure routes. Table S3 in the ESI† shows the crystal structure data obtained here for the $CaCdTi_2O_6$ compound in the $Pmc2_1$ space group.

4 Conclusions

In the search for new stable ferroelectric compounds, we have probed Ca substituted by Cd in RP1, RP2, and DP structures *via* theoretical *ab initio* simulations. Our results indicate that the $CaCdMn_2O_6$ DP compound is not stable at low pressures. Although the Mn-based DP could stabilize at pressures above 12 GPa, the dissociation into $CaBO_3$ + CdO + BO_2 has lower enthalpy. Therefore, it is unlikely that the DP will be metastable at ambient pressure. On the other hand, although the $CaCdTi_2O_6$ DP compound also tends to dissociate into single perovskites, our results have shown that this DP is stable above ~5.2 GPa, a much lower transition pressure than that for $CaCdMn_2O_6$. Additionally, the phonon dispersion results confirm that $CaCdTi_2O_6$ is dynamically stable at 0 GPa. Therefore, high-pressure synthesis routes could stabilize this DP system. Consequently, these finds, along with our results on spontaneous electrical polarization and polarization switch energy barriers,[7] suggest that the $CaCdTi_2O_6$ DP might be metastable and a possible new hybrid improper ferroelectric material.

Rondinelli and Fennie guidelines for constructing new DP structures state that at least one of the perovskite building blocks should have a strong tendency towards the *Pnma* space group.[25] Conversely, the stability properties found in this investigation show that the $CaCdMn_2O_6$ DP is thermodynamically unstable, even though $CaMnO_3$ stabilizes in the *Pnma* space group. In other words, the thermal stability of the DP structures depends on the balance between the relative enthalpy of both ABO_3 blocks used in their construction. For example, $CdTiO_3$ is not stable in the *Pnma* space group, and if one computes the thermal stability with this phase, the DP $CaCdTi_2O_6$ is thermodynamically stable. However, the results show the dissociation of the DP structure when the $R\bar{3}$ space group is used to simulate the $CdTiO_3$ system. Therefore, we found that if both building blocks of the DP material have a strong tendency to crystallize in the *Pnma* space group, the DP might dissociate into the single perovskites.

Cd-Based RP structures are not thermodynamically stable. The relative enthalpy of the dissociation components in the chemical reactions: $Cd_{n+1}B_nO_{3n+1} \rightarrow (n+1)CdO + nBO_2 (n = 1, 2)$ indicate that the reason for the instability lies in the enthalpy relations of the $CdBO_3$ (B = Mn, Ti) systems that present lower enthalpy difference w.r.t. the dissociation into simpler oxides. For n = 2, the lowest relative enthalpy always relates to the dissociation of RP2 into single perovskites plus rock-salt compounds. Substituting part of the Cd by Ca, as in $CaCd_2B_2O_7$, favors the formation of Ca perovskites and decreases the enthalpy difference to the RP2 structures. Therefore, the formation of the ABO_3 perovskites might indicate that the RP2 $A_3B_2O_7$ are stable. Indeed, substituting Cd by Ca in $Cd_3B_2O_7$

systems tends to decrease the enthalpy difference between the dissociated compounds and the RP2 structures. Conversely, solid solutions of the type $Ca_{3(1-x)}Cd_{3x}B_2O_7$ are stable for x values up to 0.20 for B = Mn and 0.07 for B = Ti. The stability properties of Ca-based compounds by Cd substitution provide chemical routes to control the spontaneous electric polarization of $Ca_3B_2O_7$ structures.[7]

RP1 compounds have the same stoichiometry as the forsterite mineral. Comparison between the enthalpies of Ca_2MnO_4 in these two types of structures showed that the ground state is the RP1 with space group *Acam*, in agreement with experimental results. However, for Ca_2TiO_4 the forsterite structure with space group *Pnma* has the lowest enthalpy, as shown by our theoretical results. This result may explain why RP1 Ca_2TiO_4 has not yet been synthesized. The phonon spectrum revealed that Ca_2TiO_4 is dynamically stable in the forsterite structure, and the enthalpy relations showed that Ca_2TiO_4 is thermally stable up to $\sim$3 GPa. At higher pressures, Ca_2TiO_4 dissociates into $CaTiO_3$ + CaO, in the same way as forsterite Mg_2SiO_4 dissociates into $MgSiO_3$ + MgO around 20 GPa.[29] The lower dissociation pressure could make Ca_2TiO_4 useful in high-pressure studies as a high pressure analogous of Mg_2SiO_4.

Conflicts of interest

There are no conflicts to declare.

Acknowledgements

MLM, LVCA, and HMP acknowledge funding from FAPESP, Projects 2018/07760-4 and 2019/07661-9. SSMS, PRR, AMLL, and JPA ackowledge funding from the projects UID/NAN/50024/2019, NECL under NORTE-01-0145-FED ER-022096, POCI-01-0145-FEDER-029454, POCI-01-0145-FEDER-032527, and FCT through CERN/FIS-TEC/0003/2019. PRR also gratefully thanks the UE, FSE and FCT-Portugal for FCT Grant No. SFRH/BD/117448/2016. LVCA and HMP also acknowledge support from CNPq projects 305753/2017-7 and 311373/2018-6. IPM and HMP thank support from federal government agency CAPES. The authors also acknowledge the National Laboratory for Scientific Computing (LNCC/MCTI, Brazil) for providing HPC resources of the Santos Dumont supercomputer (http://sdumont.lncc.br) and PRACE for awarding us access to Marconi 100 hosted by Cineca, Italy, which have contributed to the research results reported within this paper.

References

1 N. A. Benedek and C. J. Fennie, *Phys. Rev. Lett.*, 2011, **106**, 107204.
2 N. A. Benedek, A. T. Mulder and C. J. Fennie, *J. Solid State Chem.*, 2012, **195**, 11–20.
3 J. F. Scott and C. A. Paz de Araujo, *Science*, 1989, **246**, 1400–1405.
4 D. Damjanovic, *The Science of Hysteresis*, Elsevier, 2006, pp. 337–465.
5 M. J. Pitcher, P. Mandal, M. S. Dyer, J. Alaria, P. Borisov, H. Niu, J. B. Claridge and M. J. Rosseinsky, *Science*, 2015, **347**, 420–424.
6 R. Zhang, B. M. Abbett, G. Read, F. Lang, T. Lancaster, T. T. Tran, P. S. Halasyamani, S. J. Blundell, N. A. Benedek and M. A. Hayward, *Inorg. Chem.*, 2016, **55**, 8951–8960.
7 M. L. Marcondes, S. S. M. Santos, I. P. Miranda, P. Rocha-Rodrigues, L. V. C. Assali, A. M. L. Lopes, J. P. Araujo and H. M. Petrilli, *J. Mater. Chem. C*, 2020, **8**, 14570–14578.
8 S. N. Ruddlesden and P. Popper, *Acta Crystallogr.*, 1958, **11**, 54–55.
9 P. V. Balachandran, D. Puggioni and J. M. Rondinelli, *Inorg. Chem.*, 2014, **53**, 336–348.
10 P. Rocha-Rodrigues, S. S. M. Santos, I. P. Miranda, G. N. P. Oliveira, J. G. Correia, L. V. C. Assali, H. M. Petrilli, J. P. Araújo and A. M. L. Lopes, *Phys. Rev. B*, 2020, **101**, 064103.
11 P. Rocha-Rodrigues, S. S. M. Santos, G. N. P. Oliveira, T. Leal, I. P. Miranda, A. M. dos Santos, J. G. Correia, L. V. C. Assali, H. M. Petrilli, J. P. Araújo and A. M. L. Lopes, *Phys. Rev. B*, 2020, **102**, 104115.
12 S. S. M. Santos, M. L. Marcondes, I. P. Miranda, P. Rocha-Rodrigues, L. V. C. Assali, A. M. L. Lopes, H. M. Petrilli and J. P. Araujo, *J. Mater. Chem. C*, 2021, **9**, 7005–7013.
13 A. H. Ramadan, L. Hesselmann and R. A. De Souza, *J. Phys. Chem. Solids*, 2015, **86**, 90–94.
14 A. T. Mulder, N. A. Benedek, J. M. Rondinelli and C. J. Fennie, *Adv. Funct. Mater.*, 2013, 4810–4820.
15 P. Giannozzi, S. Baroni, N. Bonini, M. Calandra, R. Car, C. Cavazzoni, D. Ceresoli, G. L. Chiarotti, M. Cococcioni, I. Dabo, A. Dal Corso, S. de Gironcoli, S. Fabris, G. Fratesi, R. Gebauer, U. Gerstmann, C. Gougoussis, A. Kokalj, M. Lazzeri, L. Martin-Samos, N. Marzari, F. Mauri, R. Mazzarello, S. Paolini, A. Pasquarello, L. Paulatto, C. Sbraccia, S. Scandolo, G. Sclauzero, A. P. Seitsonen, A. Smogunov, P. Umari and R. M. Wentzcovitch, *J. Phys.: Condens. Matter*, 2009, **21**, 395502.
16 P. Giannozzi, O. Andreussi, T. Brumme, O. Bunau, M. Buongiorno Nardelli, M. Calandra, R. Car, C. Cavazzoni, D. Ceresoli, M. Cococcioni, N. Colonna, I. Carnimeo, A. Dal Corso, S. de Gironcoli, P. Delugas, R. A. DiStasio, A. Ferretti, A. Floris, G. Fratesi, G. Fugallo, R. Gebauer, U. Gerstmann, F. Giustino, T. Gorni, J. Jia, M. Kawamura, H.-Y. Ko, A. Kokalj, E. Küçükbenli, M. Lazzeri, M. Marsili, N. Marzari, F. Mauri, N. L. Nguyen, H.-V. Nguyen, A. Otero-de-la Roza, L. Paulatto, S. Poncé, D. Rocca, R. Sabatini, B. Santra, M. Schlipf, A. P. Seitsonen, A. Smogunov, I. Timrov, T. Thonhauser, P. Umari, N. Vast, X. Wu and S. Baroni, *J. Phys.: Condens. Matter*, 2017, **29**, 465901.
17 P. Hohenberg and W. Kohn, *Phys. Rev.*, 1964, **136**, B864–B871.
18 W. Kohn and L. J. Sham, *Phys. Rev.*, 1965, **140**, A1133–A1138.
19 R. Wentzcovitch, *Phys. Rev. B: Condens. Matter Mater. Phys.*, 1991, **44**, 2358–2361.

20 R. M. Wentzcovitch, J. L. Martins and G. D. Price, *Phys. Rev. Lett.*, 1993, **70**, 3947–3950.
21 F. Birch, *Phys. Rev.*, 1947, **71**, 809–824.
22 M. S. Senn, A. Bombardi, C. A. Murray, C. Vecchini, A. Scherillo, X. Luo and S. W. Cheong, *Phys. Rev. Lett.*, 2015, **114**, 035701.
23 E. L. da Silva, A. M. Gerami, P. N. Lekshmi, M. L. Marcondes, L. V. C. Assali, H. M. Petrilli, J. G. Correia, A. M. L. Lopes and J. P. Araújo, *Nanomaterials*, 2021, **11**, 897.
24 E. Posnjak and T. F. W. Barth, *Z. Kristallogr.*, 1934, **88**, 271–280.
25 J. M. Rondinelli and C. J. Fennie, *Adv. Mater.*, 2012, **24**, 1961–1968.
26 Y. S. Oh, X. Luo, F.-T. Huang, Y. Wang and S.-W. Cheong, *Nat. Mater.*, 2015, **14**, 407–413.
27 M. Dawber, K. M. Rabe and J. F. Scott, *Rev. Mod. Phys.*, 2005, **77**, 1083–1130.
28 E. Bousquet, M. Dawber, N. Stucki, C. Lichtensteiger, P. Hermet, S. Gariglio, J.-M. Triscone and P. Ghosez, *Nature*, 2008, **452**, 732–736.
29 E. Knittle and R. Jeanloz, *Science*, 1987, **235**, 668–670.

